Research Article

NMR IN BIOMEDICINE

Received: 18 September 2008, Revised: 5 February 2009, Accepted: 5 February 2009, Published online in Wiley InterScience: 25 March 2009

(www.interscience.wiley.com) DOI:10.1002/nbm.1382

Multislice multiecho T2* cardiac magnetic resonance for the detection of heterogeneous myocardial iron distribution in thalassaemia patients

Vincenzo Positano[a]*, Alessia Pepe[a], Maria Filomena Santarelli[a], Anna Ramazzotti[a], Antonella Meloni[a], Daniele De Marchi[a], Brunella Favilli[a], Eliana Cracolici[b], Massimo Midiri[b], Anna Spasiano[c], Massimo Lombardi[a] and Luigi Landini[a,d]

The present study investigated myocardial T2* heterogeneity in thalassaemia major (TM) patients by cardiac magnetic resonance (CMR), to determine whether is related to inhomogeneous iron overload distribution. A total of 230 TM patients consecutively referred to our laboratory were studied retrospectively. Three short-axis views (basal, medium and apical) of the left ventricle (LV) were obtained by multislice multiecho T2* CMR. T2* segmental distribution was mapped on a 16-segment LV model. The level of heterogeneity of the T2* segmental distribution, evaluated by the coefficient of variation (CoV), was compared with that of a surrogate data set, to determine whether the inhomogeneous segmental distribution of T2* could be generated by susceptibility artefacts. Susceptibility artefacts offer an explanation for the T2* heterogeneity observed in patients without iron overload. In subjects with global T2* below the lower limit of the normal, T2* heterogeneity increased abruptly which could not be explained by artefactual effects. Some segmental T2* values were below and others above the limit of normal threshold (20 ms) in 104 (45%) TM patients. Among these patients, 74% showed a normal T2* global value. In conclusion, a true heterogeneity in the iron overload distribution may be present in TM patients. Heterogeneity seemingly appears in the borderline myocardial iron and stabilizes at moderate to severe iron burden. Copyright © 2009 John Wiley & Sons, Ltd.

Keywords: iron overload; cardiac MRI; multiecho T2*; susceptibility artefacts

INTRODUCTION

Cardiac magnetic resonance (CMR) is commonly used in clinical practice for the assessment of myocardial iron overload in patients with primary and secondary haemochromatosis (1). CMR-based evaluation of myocardial iron overload is particularly important in patients affected by thalassaemia major (TM) because iron overload remains the main cause of heart failure in these patients (2). Biochemical measures of iron overload are inconsistent predictors of myocardial iron deposition (3), so an accurate, non-invasive assessment of iron overload should guide diagnosis, treatment and follow-up.

The iron, when present in an intracellular location in the form of ferritin and haemosiderin, forms focal clusters of magnetic inhomogeneity. The presence of these clusters results in a dramatic reduction in the protons' transverse relaxation time that can be assessed by spin-echo (T2) techniques or gradient-echo (T2*) techniques (4–6). T2 measurements are less influenced by susceptibility artefacts (7). Furthermore, T2* technique allows faster acquisition, avoiding artefacts due to cardiac motion. Although some preliminary studies in T2 multiecho heart imaging limited to the mid-ventricular septum have been reported (8), gradient-echo T2* technique is generally used in the clinical arena. Iron deposition is associated with a shortening of T2 and T2*, which can be assessed by CMR. The state-of-art technique uses ECG triggered gradient echo sequences, with readouts at multiple echo times, which are able to rapidly acquire a set of T2*-weighted images in a single breath-hold (9–11). The fitting of the magnitude signal intensity in T2*-weighted images with an appropriate decay model allows the measurement of T2*

* *Correspondence to: V. Positano, MRI Laboratory, Gabriele Monasterio Foundation, Via Moruzzi, 1 56124 Pisa, Italy.*
E-mail: positano@ifc.cnr.it

a *V. Positano, A. Pepe, M. F. Santarelli, A. Ramazzotti, A. Meloni, D. De Marchi, B. Favilli, M. Lombardi, L. Landini*
MRI Laboratory, G. Monasterio Foundation and CNR Institute of Clinical Physiology, Pisa, Italy

b *E. Cracolici, M. Midiri*
Department of Radiology, University of Palermo, Palermo, Italy

c *A. Spasiano*
Centro per la Cura delle Microcitemie, Cardarelli Hospital, Napoli, Italy

d *L. Landini*
Department of Information Engineering, University of Pisa, Pisa, Italy

Contract/grant sponsor: Centro per la lotta contro l'infarto Onlus Foundation.

Abbreviations used: *AHA, American Heart Association; CMR, cardac, magnetic resonance; CoV, coefficient of variation; LV, left ventricle; TM, thalassaemia major.*

in a defined anatomical region. This technique is feasible in clinical practice and has shown good inter-study and inter-scanner reproducibility (11–13). CMR acquisition is usually limited to a single measurement in the mid-ventricular septum to minimize the effect of motion and susceptibility artefacts. Thus, the $T2^*$ value measured in a single region of interest (ROI) drawn in the mid-ventricular septum is taken as representative of the $T2^*$ value for the whole heart (1,10,14,15).

The few histological studies available in the literature have detected heterogeneous iron deposition in TM patients (16–18), so it may be of interest to perform a 3D segmental measurement of the $T2^*$ assessment in the whole left ventricle (LV). Multislice, multiecho $T2^*$ CMR has been demonstrated to effectively assess the segmental distribution of $T2^*$ values in iron overloaded patients (11,12,19). Although a significant heterogeneity in $T2^*$ segmental distribution was observed in these studies, it is not yet clear if that represented true heterogeneous iron density or if it could have been generated by geometric and susceptibility artefacts.

To address this issue, we have investigated the relationship between $T2^*$ segmental heterogeneity and iron overload progression in a large patient population, in order to understand if imaging artefacts may account for inhomogeneous segmental distribution of $T2^*$ values.

MATERIALS AND METHODS

Magnetic resonance

Two hundred and thirty TM patients (95 men, age 29 ± 10 year) consecutively referred to our laboratory were retrospectively studied. Images acquired from 20 healthy volunteers (13 men, mean age 31 ± 11 year) were also used in this study to assess normal values for global and segmental $T2^*$ values, as will be described. All healthy subjects were completely asymptomatic, with no known history of any disease. Informed consent was obtained from all subjects and the Institutional Review Board approved the study. Multislice, multiecho CMR was performed by a 1.5 T MR scanner (GE Signa, CV/i), using a 4-channel cardiac phased array coil. Myocardial $T2^*$ distribution was assessed by a fast gradient echo–multiecho sequence (FA = 25°, matrix = 256×192, FOV = 35×35 cm, thickness = 8.0 mm, NEX = 0.75) with ECG triggering. Each slice was acquired at nine echo times (from 2.2 to 20.3 ms, with echo spacing of 2.26 ms) in a single end-expiration breath-hold to assure image alignment. Acquisition time for each slice ranged from 10 to 18 s depending on heart rate. Three short-axis views (basal, medium and apical) of the LV were acquired for each subject, following the American Heart Association (AHA) recommendations (20). A more detailed description of the acquisition sequence is provided in Reference (19).

Image analysis

Acquired images were analysed using a previously validated, custom software (HIPPO MIOT®) (19) by expert CMR operators. The software is able to map the myocardial $T2^*$ distribution into a 16-segment LV model according to the AHA standardized myocardial segmentation (20). The inter-study, intra-observer and inter-observer variabilities of the proposed methodology were previously assessed (12). Briefly, for each short-axis slice, the endocardial and epicardial contours of the LV wall were manually traced in an image corresponding to the first or second echo time. A reference point in the anterior septal insertion of the right ventricle was also defined. The two contours and the reference point were automatically replicated along all the multi-echo images. The myocardium defined in the previous step was automatically segmented into equiangular segments starting from the reference point. Six segments were used in the basal and medium slices, and four were used in the apical slice. For each segment, the mean value of the signal intensity along all TE values was calculated. The calculated decay curve was fit to the exponential model:

$$S = S_0 \exp\left(-\frac{\mathrm{TE}}{T2^*}\right) \quad (1)$$

where S represents the mean signal intensity, S_0 is a constant, $T2^*$ is the relaxation time and TE represents the echo times. Decay curve fitting was performed by Levenberg–Marquadt method and the $T2^*$ value for the segment was obtained. Figure 1 shows a typical decay curve and the resulting fitting operation. It should be noticed that the signal decay is not purely exponential, hence the adopted decay model may be affected by measurement errors. A small signal offset, almost constant over TEs, could be present due to Rician distributed MRI noise and signal from slow relaxing species as oxygenated blood (19,21). In high iron overloaded subject, the later TEs were manually excluded from the analysis to take this aspect into account. A valid alternative approach is to add a constant offset to the exponential curve, with the advantage of a reduced user-dependent variability (21). However, the later approach may not be optimal at high $T2^*$ values due to the incorrect estimation of the offset value (19). Moreover, the signal decay is modulated by a sinc function due to the susceptibility differences between tissues (22). As showed by Ghugre *et al.* (21), the fitting error induced by this effect is very small (less than 1.5%) and was further reduced in our approach, thanks to the choice of a TE interval equal to half of the period of fat-water 'beating'. To summarize, a single-exponential, ROI-based decay model was used in this study due to its robustness and its invariance to decay rate, as also suggested by other studies

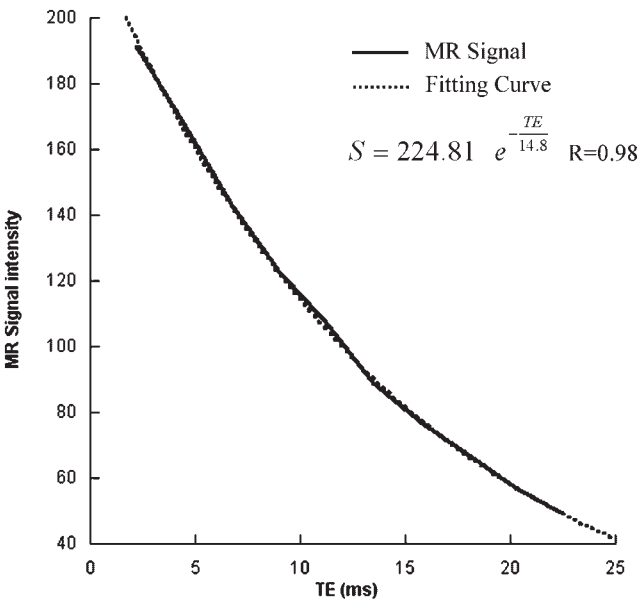

Figure 1. Typical signal decay curve ($T2^* = 14.8$ ms) and fitting curve evaluated by the single exponential model in eqn (1).

NMR IN BIOMEDICINE

(23,24). Finally, the global T2* value was obtained by averaging segmental T2* values.

Artefact modelling

Large cardiac veins and heart–lung interface represent the main artefactual sources that could affect the T2* distribution. Large cardiac veins produce perturbations of the *z*-component of the magnetic field due to the susceptibility difference between the deoxygenated blood in the vein and the surrounding tissue (25). Artefactual alterations of the T2* value are related to magnetic field perturbation in a complex way, but it is visually apparent that artefacts originate from large cardiac veins and that the effect of these artefacts rapidly decreases with the distance from the source. Figure 2 shows typical susceptibility artefacts at the basal (Fig. 2A), medium (Fig. 2B) and apical (Fig. 2C) levels. Since the susceptibility artefact intensity has a nonlinear dependence on the angle between the axis of the vein and the acquired slice, susceptibility artefacts' strength is expected to randomly vary in the population of imaged subjects. Hence, the artefact strength on a segment could be modelled as a random value extracted from a Gaussian distribution. The mean and SD of the Gaussian distribution can be evaluated on a homogeneous group of subjects as the systematic bias and the SD of measured T2* segmental values, respectively.

Heart–lung interface is another possible source of artefacts, as shown by means of qualitative analysis of pig hearts *in vivo* and *ex vivo* (26). These artefacts were less important in human studies when measurements were performed in end-expiratory breath-hold (as in this study) when phrenicomediastinal recess diminished (27). Artefacts related to this source should involve a larger area with respect to 'spot-like' artefacts similar to the ones produced by cardiac veins. Figure 2D shows a typical artefact induced by the heart–lung interface. These artefacts could affect T2* measurements in the lateral wall and might be more severe in the apical region as compared with the base and the mid-ventricular level.

We hypothesize that susceptibility artefacts are additive in the R2* (1/T2*) domain and independent of the R2* value (7). This assumption will be discussed below.

The main objective of this study is to understand if the segmental heterogeneity of T2* values measured in the patient

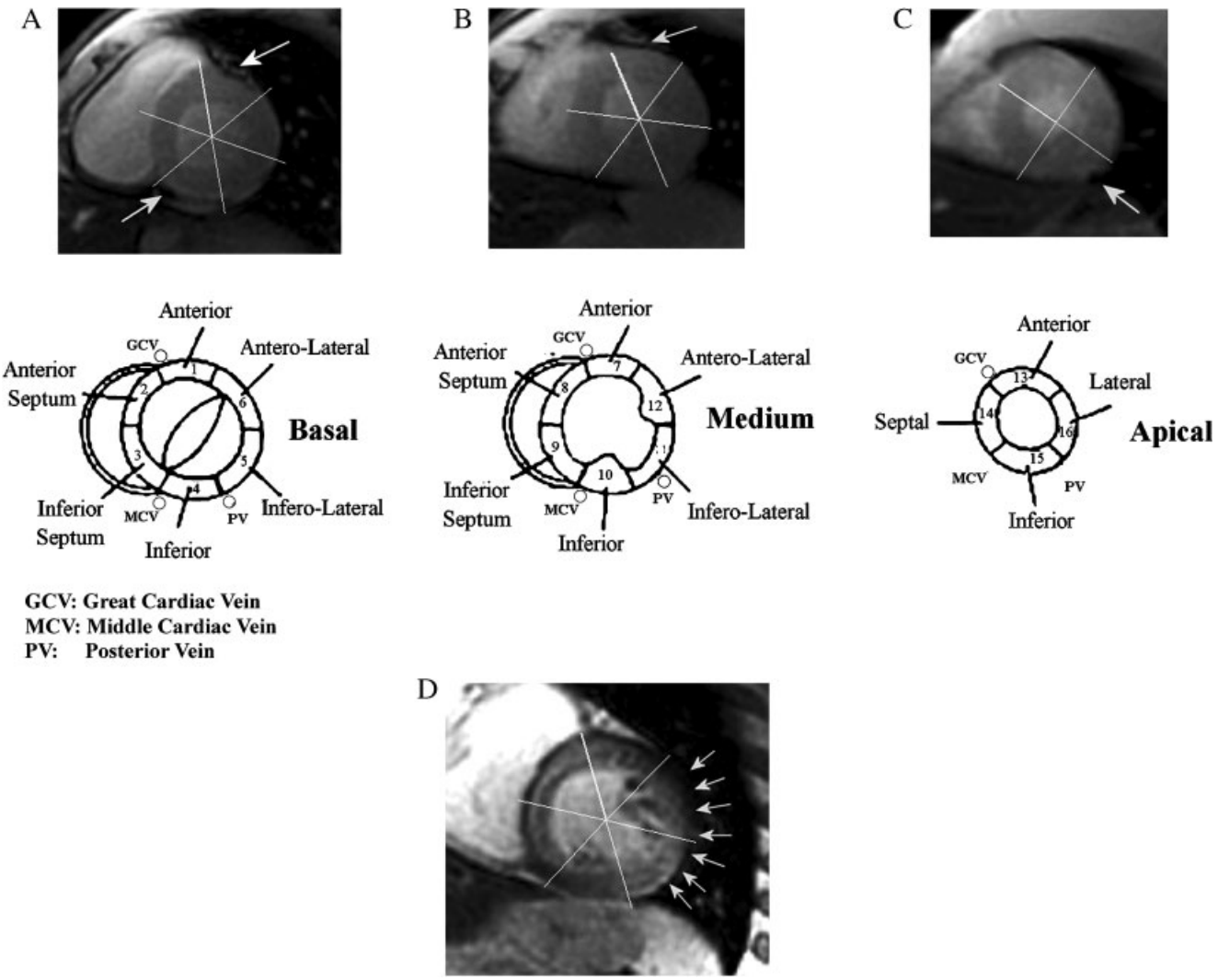

Figure 2. Mapping of segmental T2* distribution on the 16-segments model. Sources of typical artefacts: cardiac veins (A, B, C) and heart–lung interface (D).

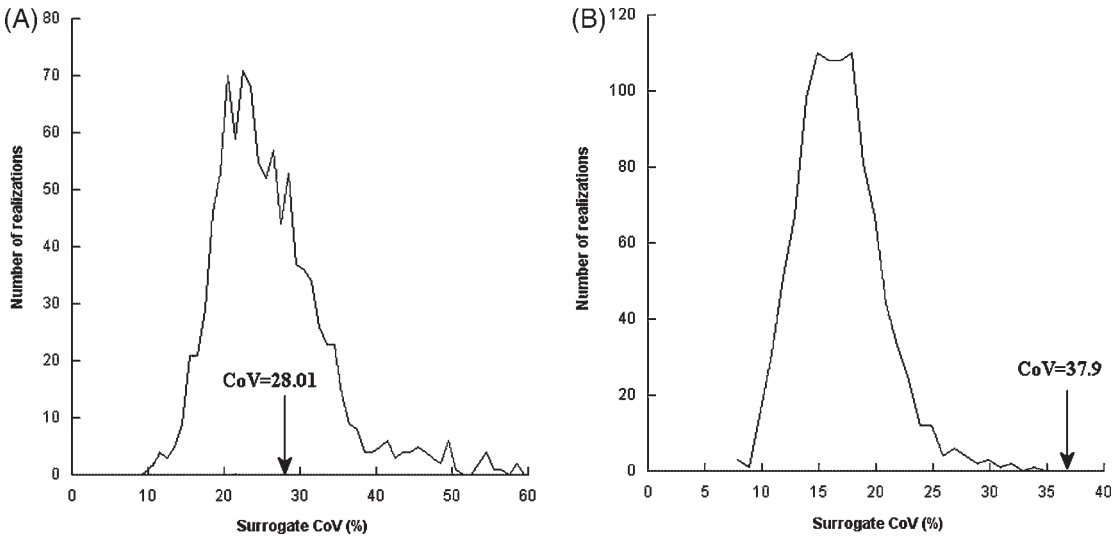

Figure 3. Examples of surrogate data realizations. (A) Patient 190 (global $T2^* = 37.8$ ms). The CoV measured on real patient data (28.01%) is well inside the mean $\pm$ 2SD window defined by surrogate data. (B) Patient 100 (global $T2^* = 26.6$ ms). The CoV measured on real patient data (37.9%) is outside the mean $\pm$ 2SD window defined by surrogate data.

population could be entirely explained by artefactual sources. A surrogate data set was obtained with the hypothesis that heterogeneous iron deposition does not exist and variations in $T2^*$ values are associated only with the effect of susceptibility artefacts. Since these artefacts are additive in $R2^*$ space, it is convenient to generate data in the $R2^*$ domain. Based on these assumptions, the $R2^*$ value $R2^*(p, s)$ in a segment s for a patient p could be modelled by adding the artefacts effect to the global $R2^*$ value $R2^*_G(p)$:

$$T2^*(p,s) = \frac{1000}{R2^*(p,s)} = \frac{1000}{R2^*_G(p) + \Delta_{R2*}(s) + \sigma_{R2*}(s)N(0,1)} \quad (2)$$

where s was the segment location, and $\Delta_{R2*}(s)$ and $\sigma_{R2*}(s)$ were the mean and the SD of the difference between $R2^*$ values in the segment s and the global LV value, respectively. $N_{0,1}(s)$ represents a normal distribution. $\Delta_{R2*}(s)$ and $\sigma_{R2*}(s)$ could be evaluated on a population of normal subjects without iron overload. In this population, the 'true' $R2^*$ value in the entire myocardium is constant; the segmental variations are due only to susceptibility artefacts.

Statistical analysis

The level of heterogeneity of the $T2^*$ segmental distribution on each patient was evaluated by calculating the coefficient of variation (CoV) as the standard deviation of the absolute value of the differences between the segmental $T2^*$ values and the global $T2^*$ value divided by the global $T2^*$ value and expressed as a percentage.

Segmental data analysis

Patient data were analysed by the Monte Carlo simulation method. For each patient involved in the study, a set of surrogate data were randomly generated using eqn (2): $R2^*_G(p)$ equal to the global $R2^*$ value measured in the subject's whole LV, $\Delta_{R2*}(s)$ and $\sigma_{R2*}(s)$ obtained from the analysis of normal subjects and random values from the Gaussian distribution $N_{0,1}(s)$ obtained by the Box–Muller method implemented in IDL 6.0 (28). One thousand surrogate data realizations were generated for each patient to simulate the $R2^*$ variations that could be associated with different distributions of artefact sources. The level of heterogeneity for each surrogate data realization was evaluated by computing the CoV as previously described.

The CoVs evaluated over the population were plotted *versus* the global $T2^*$ value. Furthermore, for each patient the mean CoV value from the surrogate data was plotted together with the mean $\pm$ 2SD. In the resulting plot, the region outside the mean $\pm$ 2SD interval represented the CoV values that could not be explained by susceptibility artefacts (probability less than 5%). Figure 3 shows typical examples of surrogate CoVs' distribution in two patients.

In clinical practice, presence of iron overload in heart is routinely assessed by comparing the measured $T2^*$ value with the normality threshold. A $T2^*$ normality threshold of 20 ms (50 Hz for $R2^*$) is commonly used in the literature (10). In the segmental analysis, the number of heart segments below the normality threshold could be used as an index of iron overload heterogeneity (12). Hence, the number of segments with an $R2^*$ value higher than the normality threshold was counted in all patients and in the relevant surrogate data, generated as previously described. Surrogate data were used to define the expected number of non-normal segmental $T2^*$ values generated by the artefacts.

Due to the heterogeneous effect of susceptibility artefacts on different heart regions, the use of a unique normality threshold for all LV segments may not be adequate. The use of an $R2^*$ segmental correction map, evaluated on a normal subject, was proposed to overcome this drawback (19). To evaluate the effectiveness of the correction technique, the number of segments with a $T2^*$ value above the normality threshold was also assessed in patients' data corrected by the procedure described in Reference (19).

NMR IN BIOMEDICINE

Table 1. Distribution of segmental R2* values in normal subjects

Segment No.	Segment	R2* Mean (Hz)	Δ_{R2^*} (Hz)	R2* SD (σ_{R2^*}) (Hz)
	Global left ventricle value	29.3	0	3.1
1	A, Anterior (basal)	32.0	2.7	7.9
2	AS, Antero-septal (basal)	26.6	−2.7	5.0
3	IS, Infero-septal (basal)	26.4	−2.9	3.8
4	I, Inferior (basal)	35.1	5.8	8.2
5	IL, Infero-lateral (basal)	30.7	1.4	5.9
6	AL, Antero-lateral (medium)	25.0	−4.3	6.6
7	A, Anterior (medium)	34.3	5.0	6.5
8	AS, Antero-septal (medium)	27.6	−1.7	5.4
9	IS, Infero-septal (medium)	27.1	−2.2	7.0
10	I, Inferior (medium)	32.0	2.7	6.3
11	IL, Infero-lateral (medium)	28.0	−1.3	6.3
12	AL, Antero-lateral (medium)	28.6	−0.7	3.7
13	A, Anterior (apical)	33.5	4.2	6.7
14	S, Septal (apical)	25.1	−4.2	5.1
15	I, Inferior (apical)	27.1	−2.2	7.0
16	L, Lateral (apical)	29.5	0.2	6.6

Mean segmental R2* values were obtained by averaging over 20 subjects; (Δ_{R2^*}) mean difference between the segmental value and the global LV value; (R2* SD) standard deviation of the distribution of R2* values among subjects.

RESULTS

Table 1 shows $\Delta_{R2^*}(s)$ and $\sigma_{R2^*}(s)$ values measured on the 20 healthy subjects involved in the study. The mean global R2* value in normal subjects was 29.3 ± 3.1 Hz. The resulting limit of the normal (mean − 2SD, $p = 0.05$) for global R2* was 35.3 Hz. The corresponding values for T2* were 36.1 ± 4.4 and 27.3 ms, respectively. Mean R2* and T2* values in the mid-ventricular septum of normal subjects were 27.3 ± 5.0 Hz and 38.5 ± 7.1 ms, respectively. The cut-off values were 37.3 Hz and 24.3 ms. A threshold of 20 ms (50 Hz), widely used in the literature, was taken as a 'conservative' cut-off value for the normal subjects.

Sixty-nine (30%) TM patients showed both mid-ventricular and global T2* values less than the normality threshold (20 ms), while 151 (66%) TM patients had both values in the normal range (>20 ms). Ten (4%) TM patients had discordant mid-ventricular and global T2* values. In 45 (20%) TM patients, the T2* values in all left ventricular segments were below 20 ms, and in 81 (35%) TM patients, the T2* values in all segments were normal. In 104 (45%) TM patients, some segmental T2* values were below and others above 20 ms; so segmental T2* values were heterogeneous with respect to the normal threshold. Of the 104 TM patients with heterogeneous T2* values, 77 (74%) showed a normal T2*global value (Fig. 4). Bland Altman plots comparing T2* values in the 16 LV segments with the global T2* values are depicted in Fig. 5.

Results of the Monte Carlo simulation for CoV analysis are shown in Fig. 6. TM patients were sorted using the global T2* value. The CoV of all the patients (square markers) and the mean CoV value averaged over 20 samples window (black line) are plotted *versus* the global T2* value. For the surrogate data, the mean CoV value (grey line) is shown together with the region inside the mean ± 2SD limits (grey dotted lines). The mean and the normal lower limit of the T2*global values assessed in the healthy subjects are shown as well (vertical black arrows).

Results of the Monte Carlo simulation for non-normal heart segments are shown in Fig. 7. The number of non-normal segments for all patients averaged over 20 samples window (black line) is plotted *versus* the global T2* value. For the surrogate data, the mean number of normal segments (grey line) is shown together with the region inside the mean ± 2SD limits. The black dotted line represents the number of non-normal segments averaged over 20 patients for the data corrected using Table 1.

DISCUSSION

Iron overload distribution in the heart has been assessed in a few studies. *Ex vivo* histological analysis revealed a 'patched' distribution of iron (16,17). Ghugre (18) compared *in vivo*, *in situ* and *in vitro* R2* segmental measurements with iron quantitation in a single, heavily iron overloaded heart (T2* in mid-ventricular septum of 3.4 ms). A 12-segments (4 basal, 4 medium and 4 apical) LV model was employed in that study. Circumferential variations of the iron distribution were noted with a very high slice-to-slice reproducibility. A CoV of 16% was assessed by histological analysis and confirmed by R2* *in vitro* measurements. R2* variability was higher *in situ* compared to *in vitro* measurements, but a numerical value of *in situ* CoV was not reported. Segmental R2* CoV in our patient population, which was afflicted with heavy iron overload, was about 23% (Fig. 6), compatible with the findings of the Ghugre study.

Several CMR studies were performed on patients with primary and secondary haemochromatosis, but almost all were limited to mid-ventricular septum measurements (9,10,29). Circumferential R2* variations were detected in a single mid-papillary slice on 48 TM patients with myocardial iron overload by Ghugre *et al.* (21). Segmental assessment of the T2* distribution in the heart was

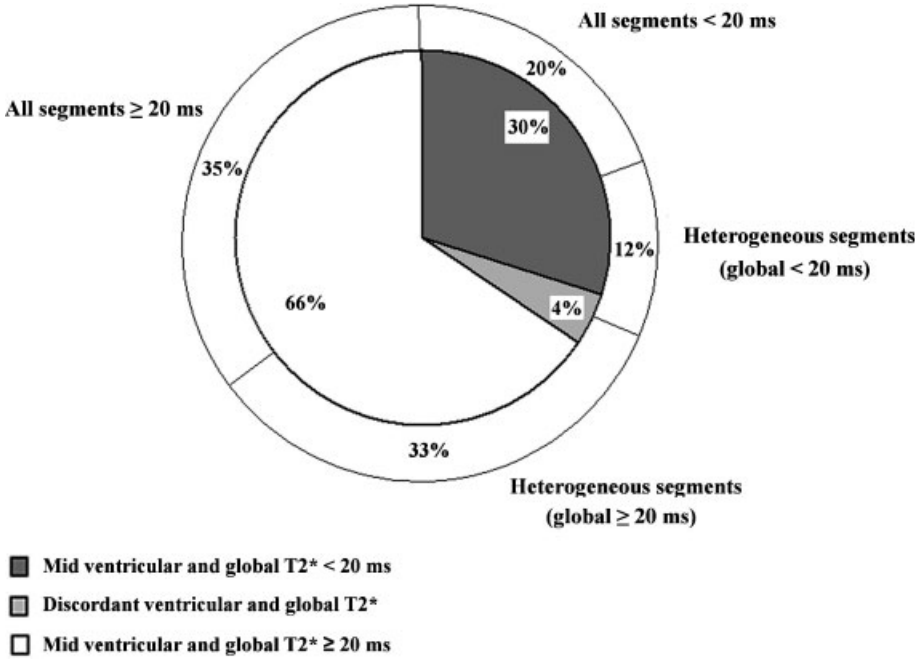

Figure 4. Homogeneous and inhomogeneous segmental distribution of $T2^*$ values in patient population. A large percentage (45%) of patients have heterogeneous segmental $T2^*$ distribution, associated with both normal and non-normal global $T2^*$ values.

performed by Pepe *et al*. (11) (53 TM patients) and was related to the efficacy of chelation agents (12) (36 TM patients).

In this study, we involved a large TM patient population (230 subjects) to obtain a statistically significant mapping of $T2^*$ heterogeneity in the whole range of $T2^*$ values exploited in clinical practice.

The main hypothesis underlining this study was that the segmental CoV measured on the patient population was generated by only the uneven iron distribution and additive susceptibility artefacts. $T2^*$ measurement errors could also play a role, producing different segmental $T2^*$ values even for subjects with exactly the same theoretical $T2^*$ value in all segments. A mean inter-observer variability (different observers in different sessions) of 12% for segmental analysis was assessed in previous studies (11,12). This value could be used as a conservative threshold for the measurement error that may affect the value used in this study, where the same observer assessed segmental values on each patient in the same session. Measurement errors affected both TM patients and surrogate data parameters (that were obtained from measurements on normal subjects). Hence, it should be expected that CoV measured in both TM patients and surrogate data were slightly overestimated. Finally, the acquisition technique used in the present study (i.e. the chosen echo times) is optimized for measurements in the abnormal range of $T2^*$ values, leading to a decrease of measurement errors at high iron overload level (11,30). Consequently, the overall finding of the study (i.e. the CoV increased below the lower limit of normal) is unlikely to be affected by this factor.

It could be argued that some non-additive artefactual sources (as geometrical artefacts generated by heart–lung interface) may play a role in CoV assessment. The effect of these non-additive artefacts should be visible at high iron overload levels. Observation of Fig. 5 reveals that the deviation of the segmental $T2^*$ values with respect to the global $T2^*$ value vanished at the low global $T2^*$ level, confirming the additive nature of the artefacts. Hence, the effect of non-additive artefacts, if any, seems to be marginal in $T2^*$ measurements. An appreciable deviation with respect to the global value at low $T2^*$ values appears only in segments 4 (basal–inferior), 7 (medium–anterior), 10 (medium–inferior) and 13 (apical–inferior). Hence these deviations, if they exist, seem to be not related to the heart–lung interface.

Another evidence of the additive nature of artefacts is that comparison between $T2^*$ and T2 measurements in heart showed that a very good linear correlation exists in iron overloaded patients ($T2^* < 20$ ms). Linear correlation is not present in patients with normal iron loading (31). Moreover, $T2^*$ assessment was demonstrated to be more reproducible in patients with high iron overload levels (10,11). The fact that the measurement error is lower at low $T2^*$ values due to the TEs used in the acquisition may partially explain this finding. However, the fitting error was demonstrated to be low for a large range of $T2^*$ values, so that the reduction of the artefact effect at high iron overload level (because the artefact became negligible with respect to high $R2^*$ values) may play a role as well. Hence, it is reasonable to model the artefact effect as an additive source with a randomly distributed strength.

From Fig. 6, it can be inferred that $R2^*$ heterogeneity for patients without iron overload was compatible with the hypothesis that the heterogeneity was generated only by additive susceptibility artefacts. In fact, CoV distribution associated with surrogate data is wide enough to include a large percentage of patient data. CoV values for TM patients with a global $T2^*$ value around 28 ms (the mean global $T2^*$ value in normal subjects) are still inside the mean $\pm$ 2SD region defined by surrogate data generation. The heterogeneity abruptly increased from 25% to about 35% near the lower normal limit of global $T2^*$ (27 ms). The maximum heterogeneity value was reached in borderline patients with a global $T2^*$ value between 20

NMR IN BIOMEDICINE

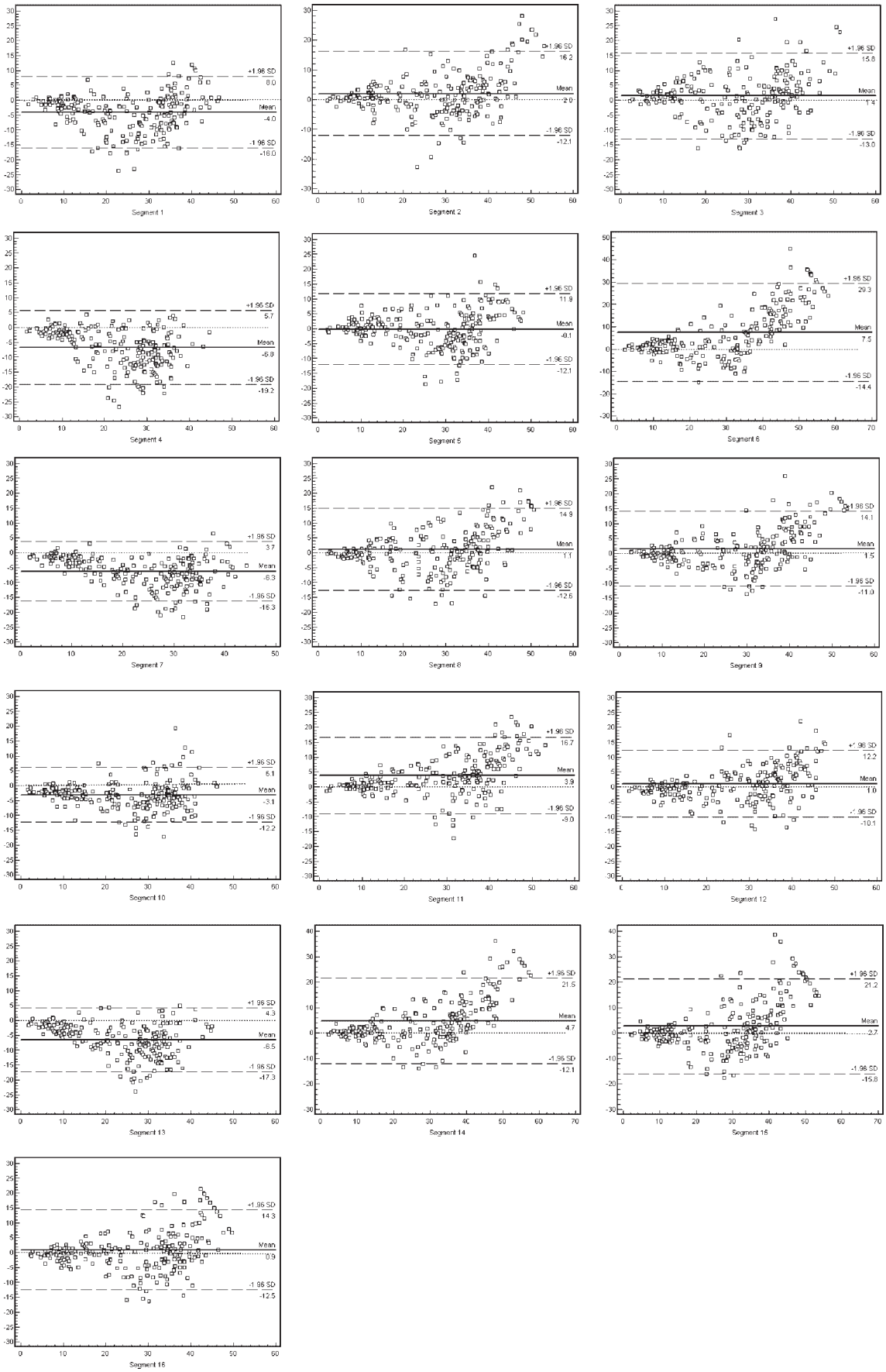

Figure 5. Bland Altman plots depicting the relationship between segmental and global T2* values.

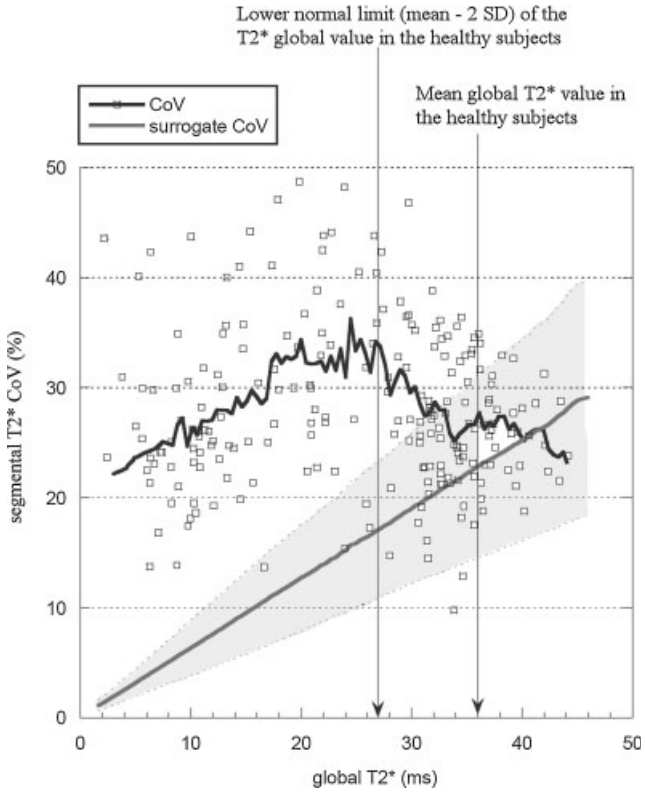

Figure 6. T2* value heterogeneity assessed by the CoV in TM patients and in the surrogate data. The white squares and the black line represent single patient measurements and the CoV average on all patients, respectively. The grey line represents the mean CoV of the surrogate data with the mean ± 2SD limits (grey dotted lines). The mean and the normal lower limit of the T2* global value assessed in the healthy subjects are shown as well (vertical black arrows).

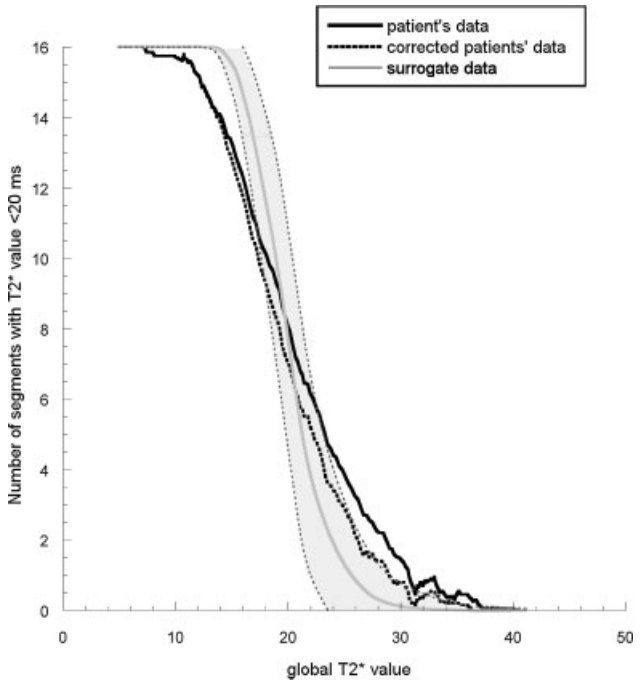

Figure 7. T2* value heterogeneity assessed by the number of heart segments below the normality threshold (20 ms) in TM patients and in the surrogate data. The solid black line represents patients' averaged measurements. The black dotted line represents the patients' averaged measurements after the correction of segmental data by the correction map in Table 1. The grey line represents surrogate data with the mean ± 2SD (grey dotted lines).

and 27 ms. Then, the heterogeneity decreased linearly, returning to 25% in patients with heavy iron overload. The CoV rate of decrease is almost the same as the rate of decrease of CoV for surrogate data.

A possible explanation of the significant CoV increase in patients with mild iron overload is that a true heterogeneity in iron overload distribution could be present in a significant percentage of TM patients. Iron overload heterogeneity could appear in the mild myocardial iron burden, justifying the strong CoV increase in borderline patients. When significant iron overload is present in all LV segments, iron heterogeneity could remain stable with the progression of disease. CoV reduction for low T2* values could be explained by the vanishing of susceptibility artefacts that are additive in the R2* space.

Iron deposition heterogeneity seems to appear in the borderline myocardial iron overload, and stabilizes for moderate to severe iron burden. Thus, it can be reasonable to use the number of LV segments with a T2* value below a normality threshold (20 ms) to monitor the evolution of myocardial iron burden (11,12). Figure 7 shows the progression of the number of non-normal segments with global LV T2* values in our population. As expected, the number of non-normal sectors smoothly increases from 0 to 16, with a mean value of 8 segments which corresponds to the normality threshold ($T2^* = 20$ ms) for the global T2* value. However, the transition range between a 'full normal' and a 'full pathological' condition is larger in the patients' data set, with respect to the surrogate data that take into account only the effect of the susceptibility artefacts. If an appropriate segmental correction map based on the values in Table 1 is applied (19), patients' corrected data are not significantly different from the surrogate data in the T2* normal range ($T2^* > 20$ ms). In both raw and corrected data, the number of non-normal segments is significantly different in patients' and surrogate data for global T2* values related to iron overloaded patients. Again, this could mean that the presence of non-normal LV segments cannot be explained by the effect of susceptibility artefacts.

In our study, a large percentage of TM patients (45%) showed an inhomogeneous segmental T2* distribution compared to the normal threshold. Out of the TM patients with an inhomogeneous segmental T2* distribution, a large percentage (74%) presented global and mid-ventricular T2* values in the normal range (Fig. 4). It is possible that segmental analysis may play a role in early and exhaustive detection of myocardial iron overload, although further studies are required to clarify this issue.

In conclusion, T2* segmental heterogeneity in TM patients shows a significant increase from a normal state to an iron overload condition. This finding cannot be explained by the effect of MRI artefacts that are additive in the R2* domain and should vanish with the progression of iron overload. The more likely interpretation is that a true heterogeneity in iron overload distribution exists in TM patients and could be detected by T2* CMR. Thus, segmental analysis may be useful in the early detection of myocardial iron overload in borderline TM patients.

Acknowledgements

We thank all the thalassaemia doctors involved in the study, in particular A. Maggio (Cervello Hospital, Palermo), P. Cianciulli (Sant'Eugenio Hospital, Roma), M. Centra (Casa del Sollievo IRCCS Hospital, San Giovanni Rotondo), V. Caruso (Garibaldi Hospital, Catania), D. Maddaloni (Engles Profili Hospital, Fabriano), and V. De Sanctis (St Anna Hospital, Ferrara). We also thank all the patients for their cooperation. A. Pepe was supported by a grant from the Centro per la lotta contro l'infarto Onlus Foundation.

REFERENCES

1. Pennell DJ. T2* magnetic resonance and myocardial iron in thalassaemia. Ann. NY Acad. Sci. 2005; 1054: 373–378.
2. Borgna-Pignatti C, Cappellini MD, De Stefano P, Del Vecchio GC, Forni GL, Gamberini MR, Ghilardi R, Origa R, Piga A, Romeo MA, Zhao H, Cnaan A. Survival and complications in thalassaemia. Ann. NY Acad. Sci. 2005; 1054: 40–47.
3. Mavrogeni SI, Markussis V, Kaklamanis L, Tsiapras D, Paraskevaidis I, Karavolias G, Karagiorga M, Douskou M, Cokkinos DV, Kremastinos DT. A comparison of magnetic resonance imaging and cardiac biopsy in the evaluation of heart iron overload in patients with beta-thalassaemia major. Eur. J. Haematol. 2005; 75: 241–247.
4. Gossuin Y, Muller RN, Gillis P. Relaxation induced by ferritin: a better understanding for an improved MRI iron quantification. NMR Biomed. 2004; 17: 427–432.
5. Ghugre NR, Coates TD, Nelson MD, Wood JC. Mechanisms of tissue-iron relaxivity: nuclear magnetic resonance studies of human liver biopsy specimens. Magn. Reson. Med. 2005; 54: 1185–1193.
6. Brooks RA, Vymazal J, Goldfarb RB, Bulte JW, Aisen P. Relaxometry and magnetometry of ferritin. Magn. Reson. Med. 1998; 40: 227–235.
7. St Pierre TG, Clark PR, Chua-Anusorn W. Single spin-echo proton transverse relaxometry of iron-loaded liver. NMR Biomed. 2004; 17: 446–458.
8. He T, Gatehouse PD, Anderson LJ, Tanner M, Keegan J, Pennell DJ, Firmin DN. Development of a novel optimized breathhold technique for myocardial T2 measurement in thalassaemia. J. Magn. Reson. Imaging 2006; 24: 580–585.
9. Wood JC, Ghugre N. Magnetic resonance imaging assessment of excess iron in thalassaemia, sickle cell disease and other iron overload diseases. Hemoglobin 2008; 32: 85–96.
10. Westwood M, Anderson LJ, Firmin DN, Gatehouse PD, Charrier CC, Wonke B, Pennell DJ. A single breath-hold multiecho T2* cardiovascular magnetic resonance technique for diagnosis of myocardial iron overload. J. Magn. Reson. Imaging 2003; 18: 33–39.
11. Pepe A, Positano V, Santarelli MF, Sorrentino F, Cracolici E, De Marchi D, Maggio A, Midiri M, Landini L, Lombardi M. Multislice multiecho T2* cardiovascular magnetic resonance for the detection of the heterogeneous distribution of myocardial iron overload. J. Magn. Reson. Imaging 2006; 23: 662–668.
12. Pepe A, Lombardi M, Positano V, Cracolici E, Capra M, Malizia R, Prossomariti L, De Marchi D, Midiri M, Maggio A. Evaluation of the efficacy of oral deferiprone in beta-thalassaemia major by multislice multiecho T2*. Eur. J. Haematol. 2006; 76: 183–192.
13. Tanner MA, He T, Westwood MA, Firmin DN, Pennell DJ. Multi-center validation of the transferability of the magnetic resonance T2* technique for the quantification of tissue iron. Haematologica 2006; 91: 1388–1391.
14. Mavrogeni S, Gotsis ED, Berdousi E, Ladis V, Verganelakis D, Toulas P, Cokkinos DV. Myocardial and hepatic T2* magnetic resonance evaluation in ex-thalassemic patients after bone-marrow transplantation. Int. J. Cardiovasc. Imaging 2007; 23: 739–745.
15. Wood JC, Tyszka JM, Carson S, Nelson MD, Coates TD. Myocardial iron loading in transfusion-dependent thalassaemia and sickle cell disease. Blood 2004; 103: 1934–1936.
16. Olson LJ, Edwards WD, Holmes DRJ, Miller FAJ, Nordstrom LA, Baldus WP. Endomyocardial biopsy in hemochromatosis: clinicopathologic correlates in six cases. J. Am. Coll. Cardiol. 1989; 13: 116–120.
17. Olson LJ, Edwards WD, McCall JT, Ilstrup DM, Gersh BJ. Cardiac iron deposition in idiopathic hemochromatosis: histologic and analytic assessment of 14 hearts from autopsy. J. Am. Coll. Cardiol. 1987; 10: 1239–1243.
18. Ghugre NR, Enriquez CM, Gonzalez I, Nelson MDJ, Coates TD, Wood JC. MRI detects myocardial iron in the human heart. Magn. Reson. Med. 2006; 56: 681–686.
19. Positano V, Pepe A, Santarelli MF, Scattini B, De Marchi D, Ramazzotti A, Forni G, Borgna-Pignatti C, Lai ME, Midiri M, Maggio A, Lombardi M, Landini L. Standardized T2* map of normal human heart in vivo to correct T2* segmental artefacts. NMR Biomed. 2007; 20: 578–590.
20. Cerqueira MD, Weissman NJ, Dilsizian V, Jacobs AK, Kaul S, Laskey WK, Pennell DJ, Rumberger JA, Ryan T, Verani MS. Standardized myocardial segmentation and nomenclature for tomographic imaging of the heart: a statement for healthcare professionals from the Cardiac Imaging Committee of the Council on Clinical Cardiology of the American Heart Association. Circulation 2002; 105: 539–542.
21. Ghugre NR, Enriquez CM, Coates TD, Nelson MDJ, Wood JC. Improved R2* measurements in myocardial iron overload. J. Magn. Reson. Imaging 2006; 23: 9–16.
22. Fernández-Seara MA, Wehrli FW. Postprocessing technique to correct for background gradients in image-based R2* measurements. Magn. Reson. Med. 2000; 44: 358–366.
23. He T, Gatehouse PD, Kirk P, Mohiaddin RH, Pennell DJ, Firmin DN. Myocardial T2* measurement in iron-overloaded thalassaemia: an ex vivo study to investigate optimal methods of quantification. Magn. Reson. Med. 2008; 60: 350–356.
24. He T, Gatehouse PD, Smith GC, Mohiaddin RH, Pennell DJ, Firmin DN. Myocardial T2* measurements in iron-overloaded thalassaemia: an in vivo study to investigate optimal methods of quantification. Magn. Reson. Med. 2008; 60: 1082–1089.
25. Reeder SB, Faranesh AZ, Boxerman JL, McVeigh ER. In vivo measurement of T2* and field inhomogeneity maps in the human heart at 1.5 T. Magn. Reson. Med. 1998; 39: 988–998.
26. Atalay MK, Poncelet BP, Kantor HL, Brady TJ, Weisskoff RM. Cardiac susceptibility artifacts arising from the heart–lung interface. Magn. Reson. Med. 2001; 45: 341–345.
27. Wacker CM, Bock M, Hartlep AW, Beck G, van Kaick G, Ertl G, Bauer WR, Schad LR. Changes in myocardial oxygenation and perfusion under pharmacological stress with dipyridamole: assessment using T2* and T1 measurements. Magn. Reson. Med. 1999; 41: 686–695.
28. Box GE, Mervin E, Muller A. A note on the generation of random normal deviates. Ann. Math. Stat. 1958; 29: 610–611.
29. Pennell DJ. MRI and iron-overload cardiomyopathy in thalassaemia. Circulation 2006; 113: f43–f44.
30. Anderson LJ, Holden S, Davis B, Prescott E, Charrier CC, Bunce NH, Firmin DN, Wonke B, Porter J, Walker JM, Pennell DJ. Cardiovascular T2-star (T2*) magnetic resonance for the early diagnosis of myocardial iron overload. Eur. Heart J. 2001; 22: 2171–2179.
31. He T, Smith GC, Gatehouse PD, Mohiaddin RH, Firmin DN, Pennell DJ. On using T2 to assess extrinsic magnetic field inhomogeneity effects on T2* measurements in myocardial siderosis in thalassaemia. Magn. Reson. Med. 2009; 61: 501–506.

